Integrating Multidimensional Feature Indices and Phenological Windows for Mapping Cropping Patterns in Complex Agricultural Landscape Regions

Haichao Yang [ID], Danyang Wang, Jingda Xin, Hao Qian, Cheng Li, Yunqi Wang, Yayi Tan, Jingyu Dai, Haiyan Zhao, and Zhaofu Li [ID]

Abstract—Acquiring a comprehensive understanding of cropping patterns and their spatiotemporal distribution is crucial for sustainable agricultural development and ecological environment protection. However, the similarity of crop spectra and the diversity of ecosystem types hinder the accurate mapping of cropping patterns, especially in agricultural landscape regions. Hence, taking Xinghua County as study area, this article proposed a novel method for integrating multidimensional feature indices and phenological windows, named phenological window feature (PWF), to achieve efficient and accurate mapping of cropping patterns. In this study, we adopt a two-step approach. First, time-series curves of feature indices were constructed using Sentinel-1/2 satellite data to determine the phenological windows of different cropping patterns and construct PWF sets. Then, the ruleset threshold method (RTM) and random forest (RF) algorithms were used to map cropping patterns including wheat-rice, crayfish-rice, vegetable-rice, rice-rapeseed, rapeseed-vegetable, and year-round vegetables. The results indicate that the phenological windows extracted from the cropping patterns in the study area were 30–120, 90–135, and 200–270 days, respectively. The overall accuracies of RTM and RF, based on PWF, were 85.91% and 89.50%, respectively, and the kappa coefficients for RTM and RF were 0.831 and 0.872, respectively. In terms of classification performance, RF slightly outperformed RTM. The study demonstrates that PWF proposed in this article can be effectively utilized for mapping cropping patterns in complex agricultural landscape regions.

Index Terms—Cropping pattern, feature indices, Google earth engine, phenological window, Sentinel-1/2.

I. INTRODUCTION

LAND resources are an integral part of the ecosystem [1]. A growing body of research suggests that land management practices can have a significant impact on the delivery of ecosystem services at the landscape level [2], [3], [4]. Crop

rotation, as a biological measure that combines land use and land cultivation, constitutes a significant factor influencing the quality of cultivated land and crop yield [5], [6], [7]. Here, we define cropping patterns as the sequential interseasonal rotation of different crops or complex planting combinations on the same field during the year [8], [9]. However, in many regional statistical yearbooks, only information on arable land area and crop types are reported, ignoring the impact of cropping patterns on sustainable agricultural use [10]. Current research also focuses on mapping individual crop types or cropping intensity, and there is not yet a suitable method for mapping cropping patterns in agriculturally intensive regions [11], [12], [13]. As such, obtaining rapidly high-precision distribution information of cropping patterns plays a crucial role in advancing sustainable agricultural development in the region.

The rapid advancement of satellite remote sensing technology has facilitated more convenient periodic monitoring of crop cycles and provided more possibilities for mapping cropping patterns through remote sensing [14], [15], [16]. Research on mapping cropping patterns is currently primarily categorized into three types. The first involves multitemporal image change detection, relying on examining statistical measures or models to detect changes in pixels or objects across different time periods, thereby discerning crop rotation practices. For example, Ye et al. [17] proposed an unsupervised object-oriented crop rotation detection method using time-series polarimetric synthetic aperture radar data to detect crop rotation changes [17]. Ma et al. [18] utilized bitemporal-feature-difference method to map rice-crayfish fields in Sihong, achieving an accuracy of 94% [18]. This method leverages multitemporal images and a set of algorithms to rapidly obtain crop rotation information for large regions. However, such approaches often can only detect whether crop rotation has occurred or identify a single cropping pattern, potentially limiting their applicability in regions with complex cropping patterns.

Second, mapping cropping patterns through spatial overlay analysis based on mapping results of single-season crops. This method entails extracting crop types during the same growing season and integrating spatial distribution information of single-season crops into a single vector data layer, thereby deducing cropping patterns. Waldhoff et al. [19] obtained diverse crop sequences by combining annual crop maps spanning eight consecutive years, identifying dozens of representative crop

rotations [19]. However, this method relies on the accuracy of single-season crop mapping [20], and the combination of multiple independently generated crop distribution maps may result in meaningless crop sequences. This limitation restricts the practical decision-making for farmers in agricultural management.

The third category involves capturing the distinctive phenological characteristics of crops to characterize changes in the crop growth cycle and subsequently map cropping patterns. This represents the current mainstream direction in the mapping of cropping patterns [10], [21], [22]. Currently, research is primarily categorized into two approaches. The first method is to utilize the threshold of a certain feature of VIs at a certain time node in the time series curve, such as the peak, the amplitude of the growing season, and the maximum slope of change value. This is then combined with a dedicated decision tree or rule set to map cropping patterns. For example, Chen et al. [14] employed NDVI time series data to formulate five temporal indices, and established a decision set with optimized thresholds to categorize cropping patterns in the Mato Grosso state of Brazil, attaining an overall accuracy of 73% [14]. Liu et al. [9] utilized the maximum value, the average value of the growth duration, and the coefficient of variation of the seasonal amplitude in the EVI time series curve to calculate flooding frequency, cropping intensity, cropping diversity, and coefficient of variation, and partitioned the cropping patterns into nine subsystems subsequently [9]. This approach underscores the importance of selecting appropriate time points and threshold during the crop growth cycle to map cropping patterns, yielding relatively high accuracy. However, due to the subjective nature of threshold selection, it will be a challenge when directly applying this method to extensive geographical areas, particularly in regions with insufficiently detailed ground observations. Second, methods based on supervised classification. The selection of suitable feature variables and classifiers is important to map cropping patterns. Liu et al. [23] collaborated on optical and SAR time series, extracting time features and the growing characteristics of the rotation systems, and employed a hybrid deep learning architecture to discern the rice rotation pattern in Hunan Province [23]. Li et al. [4] utilized the peak and valley quantity characteristics in the NDVI time series curves of double-cropping rice, single-cropping rice, and winter wheat during the overwintering period, and mapped the spatial distribution of single-cropping rice, double-cropping rice, and rice-wheat rotation, using random forest models and decision rule models [24]. This process also found that the random forest-based model is more suitable for mapping crops in multiple growing seasons. This conclusion aligns with the findings of Tariq et al. [16]. However, these studies also revealed that different crops with similar phenological periods may display similar characteristics. Additionally, the time points for distinguishing the same crop, influenced by variations in crop sowing times, may be inconsistent. Thus, models relying on decision rules may face challenges in effectively detecting differences, resulting in a relatively lower accuracy in the extracted information. Furthermore, some studies like [25] and [26] contend that integrating multiple features, such as SAR images and elevation, proves advantageous in effectively characterizing
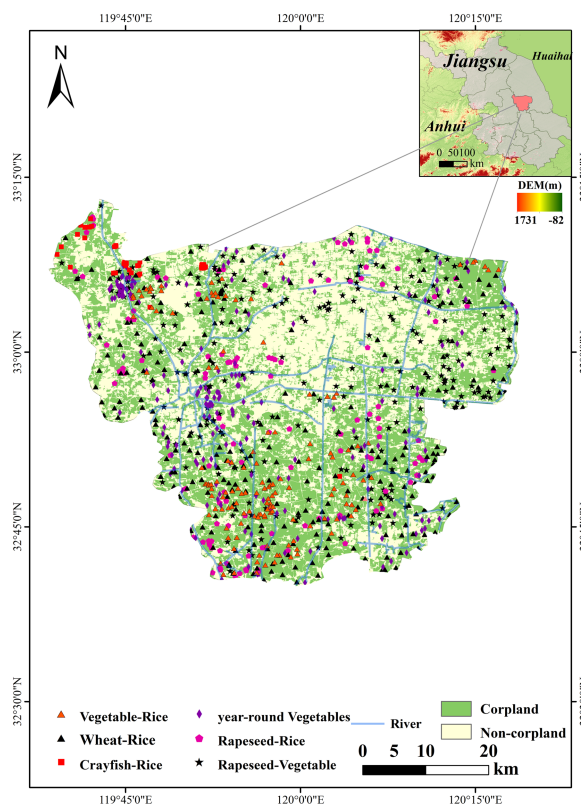

Fig. 1. Study and samples.

distinct differences among various crops, which improves the accuracy of mapping cropping patterns, consequently.

In summary, the selection of suitable time nodes and characteristic variables proves advantageous in the mapping of cropping patterns. Thus, this study proposed a method that integrates multidimensional feature variables and optimal phenological windows to map cropping patterns distribution, using radar and optical data from S1 and S2, and explored its applicability in agriculturally intensive areas by the currently popular threshold method and random forest method.

II. MATERIAL AND METHODS

A. Study Area

Xinghua County is located in the center of the Lixia River Sag in the Jianghuai Plain (32°44′N–33°16′N, 119°43′E–120°16′E) (see Fig. 1). The county covers an area of 2393.35 km² and belongs to the north subtropical humid monsoon climate, with four distinct seasons, simultaneous rain and heat, rich water resources, and superior farming conditions. The area has a high level of agricultural intensification and complex cropping patterns and the main crops are rice, wheat, and rapeseed, with a typical cropping structure of two cropping seasons per year. In addition, the total scale of local vegetable cultivation is large, including chives, Longxiang taro and cabbage, etc. There are many types of vegetables, but all of them have smaller scales compared to the main crops. Therefore, in this article, they will be uniformly classified as a single class of vegetables for analysis. Xinghua County, with a water area of nearly 1.2 million mu,

TABLE I
CROP CALENDARS OF MAJOR CROPS IN THE STUDY AREA

Month	Oct			Nov			Dec			Jan			Feb			Mar			Apr			May			Jun			Jul			Aug			Sep		
Ten days	F	M	L	F	M	L	F	M	L	F	M	L	F	M	L	F	M	L	F	M	L	F	M	L	F	M	L	F	M	L	F	M	L	F	M	L
Wheat																																				
Rapeseed																																				
Rice																																				
Taro																																				
Chives																																				

is known for its rich aquatic resources and is often referred to as the "Land of Fish and Rice." In recent years, the scale of crayfish-rice co-cropping as an emerging farming model in the study area has been increasing. The cocropping process can be divided into two stages, the rice planting stage from the beginning of June to the beginning of November, and the irrigation and soaking stage for the rest of the time [18]. In summary, the cropping patterns of the study area can be divided into six cropping patterns: wheat-rice, crayfish-rice, vegetable-rice rapeseed-rice, rapeseed-vegetable, and year-round vegetables. The crop calendars of the study area are shown in Table I.

B. Sentinel-1 SAR GRD and Sentinel-2 MSI Data

The S1 SAR GRD data adopts the VH (vertical transmit/horizontal receive) cross-polarization method under the interferometric wide swath mode. Its advantage is that it is not affected by clouds and rain, and the revisit cycle is short [27]. S1 SAR GRD data in the GEE (Google Earth Engine) platform has been preprocessed by past thermal noise and radiation calibration. Because of the influence of different polarization methods on the backscattering coefficient [28], combined with the study area, this study selected the S1 VH polarization data in 2020 and converted it into the backscattering coefficient.

The S2 MSI optical remote sensing data are Level-2A products that have undergone atmospheric correction and geometric correction. There are 13 bands in total, ranging from visible light to near-infrared and short-wave infrared bands, with a spatial resolution of 10–60 m and a temporal resolution of about 5 days [29]. Its built-in quality assessment band has identified cloud pixels [30]. In this study, the S2 image data with cloud cover less than 30% of the study area in 2020 were selected, and preprocessing such as cloud removal was performed, and the spatial resolution was uniformly resampled to 10 m.

C. Ground Reference Data

Combining the field survey results with the historical images of 2020 on Google earth to select samples, the sample information is as follows: 241 sample points of rice-wheat, 44 sample points of rice-crayfish, 139 sample points of vegetable-rice, 120 sample points of rape-rice, 224 sample points of rape-vegetable, 193 sample points of annual vegetables, and 88 sample points of other cropping patterns (including rape-soybean, rape-corn, single-season fallow), which are divided into categories 1–7 according to the above order, and a total of 1049 sample points (see Fig. 1).

To exclude the interference of nonvegetated land cover types such as built-up areas on sample selection. In this study, preselected sample points of various ground objects were used to train the RF classifier for land use classification in the study, which included five types: cultivated land, forest, water, building, and others. The noncultivated land areas were then masked out to focus on the cultivated layer for mapping cropping patterns.

III. METHODOLOGY

In this study, the phenological window feature (PWF) was proposed to create a new feature. The crux of constructing PWF involved selecting classification features and determining phenological windows (number and period of windows). The specific approach was as follows: initially, chosen appropriate features and built a time series curve to observe the distinct differences between different cropping patterns. Then, determined the number of windows and their periods following phenological window division rules. Finally, employed RTM and RF methods to validate the classification effectiveness of PWF and mapped the cropping patterns in the study area (Fig. 2). PW1, PW2, and PW3 represent phenological windows 1, 2, and 3.

A. Index Calculation and Time-Series Construction

Time-series analysis of crop phenology is the basis for mapping cropping patterns [31], [32]. In this study, we used the NDVI, EVI, LSWI, RVI, and VH time series curve of representative training samples to identify crop phenological features and reflect crop growth process, such as sowing, seedlings, heading, maturation and harvest within a year. In order to analyze the overall trend and express the effect, we calculated the average value of VIs and VH obtained during half a month to develop a
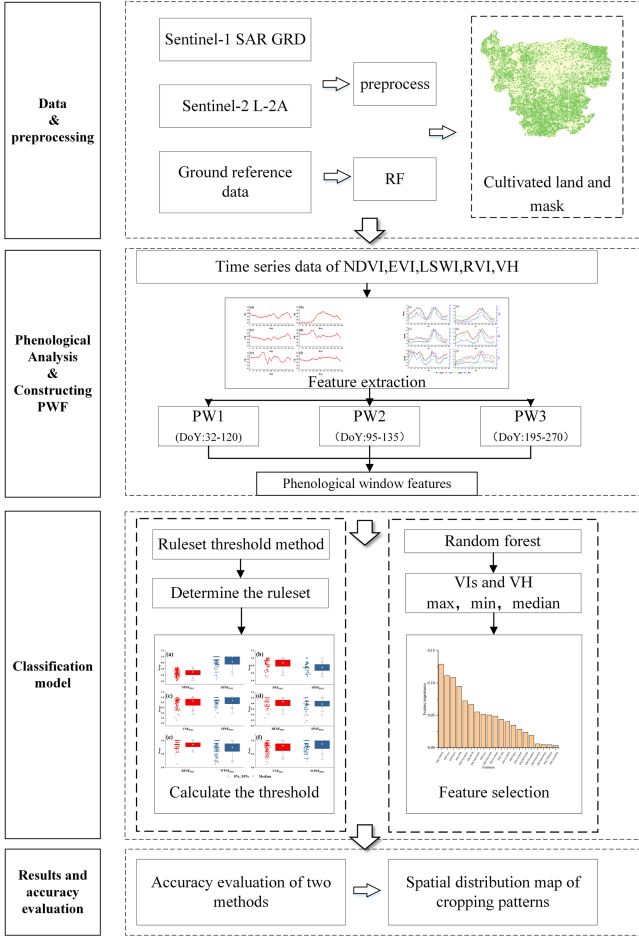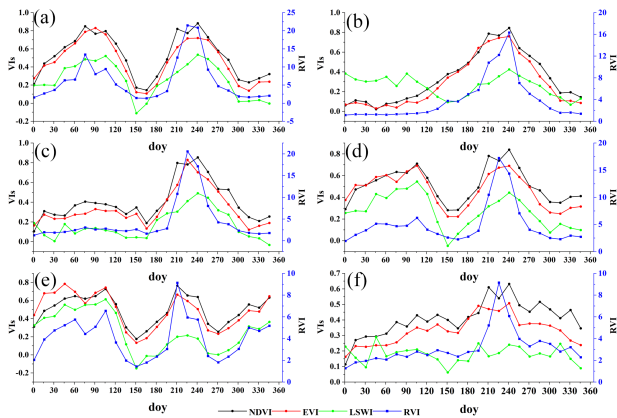
Fig. 2. Workflow of the study.

Fig. 3. VIs spectral curves of main cropping patterns. (a) Wheat-rice. (b) Crayfish-rice. (c) Vegetable-rice. (d) Rice-rapeseed. (e) Rapeseed-vegetable. (f) Year-round vegetables.

half-month composite image (see Figs. 3 and 4). The calculation formula of VIs is as follows:

$$\text{NDVI} = \frac{B_8 - B_4}{B_8 + B_4} \tag{1}$$

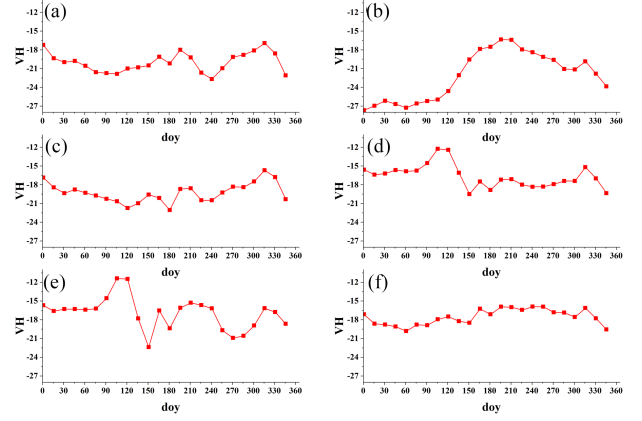$$\text{EVI} = 2.5 \times \frac{B_8 - B_4}{B_8 + 6 \times B_4 - 7.5 \times B_2 + 1} \tag{2}$$

Fig. 4. VH curves of main cropping patterns. (a) Wheat-rice. (b) Crayfish-rice. (c) Vegetable-rice. (d) Rice-rapeseed. (e) Rapeseed-vegetable. (f) Year-round vegetables.

$$\text{LSWI} = \frac{B_8 - B_{11}}{B_8 + B_{11}} \tag{3}$$

$$\text{RVI} = \frac{B_8}{B_4} \tag{4}$$

where the B_2, B_4, B_8, and B_{11} represent the blue band, the red band, the near infrared band, and the short wave infrared, respectively.

B. Phenological Window Determination

Each crop exhibits unique phenological features during the planting, growing, and harvesting stages, which offer the opportunity to utilize remote sensing time series images for mapping different cropping patterns [33]. In this article, we named this unique feature that different crops exhibit within their specific growth stages as the PWF. Therefore, it is important to express this feature with an appropriate index and capture this specific time window. The determination of the phenological window involves three steps. First, identifying the features that can differentiate a specific crop from others during its growth period. Second, determining the time window in which these features persist, which means that finding the starting point and the end point of the feature difference, respectively, similar to finding the SOS and EOS of the crop growth cycle. Last, merging similar time windows while preserving the differences in features within the same window.

Based on the above definitions, we performed a brief analysis of Figs. 3 and 4 to determine the phenological window. Among winter crops, wheat exhibits a higher NDVI value at 60–120 days compared to rapeseed and vegetables during the same period. Vegetables, on the other hand, show a significantly smaller RVI value at 1–120 days compared to wheat and rapeseed during the same period. Moreover, rapeseed demonstrates a higher VH value at 1–140 days compared to other crops, with a more pronounced difference at 90–135 days. During the summer and autumn cropping seasons, rice exhibits a higher NDVI value at 200–270 days compared to vegetables during the same period. Furthermore, NDVI and EVI values are generally higher than

TABLE II
CHARACTERISTIC SIGNAL COMBINATIONS FOR DIFFERENT CROPPING PATTERNS

phenological window	PW1	PW2	PW3
Rice-Wheat	SPS	/	SPS
Rice-Crayfish	FS	/	SPS
Rice-Vegetable	VS	/	SPS
Rice-Rapeseed	/	RFS	SPS
Rapeseed-Vegetable	/	RFS	WPS
year-round Vegetables	VS	/	WPS

LSWI during the growth of crops. However, in the case of crayfish-rice cocropping in flooded fields, NDVI and EVI values are smaller than LSWI, and VH values from 1 to 150 days are also significantly lower compared to other crops during the same period. Based on the analysis, the determined time windows for this study were 30–120, 1–120, 90–135, and 200–270 days, respectively. During the process of merging similar time windows, it was observed that combining the time windows of 30–120 and 1–120 days into 30–120 days did not result in a decrease in the differences in characteristics. However, merging the time window for rape recognition into 90–120 or 30–120 days resulted in a significant reduction in feature variance. Based on the principle of determining the phenology window, this study classified the time window of 30–120 days as PW1 (phenology window 1), 90–135 days as PW2, and 200–270 days as PW3.

C. RTM Model

The PWF of different cropping patterns exhibit distinct characteristic differences within phenological windows. In this study, these characteristic differences were utilized as characteristic signals, and the combination of characteristic signals from different cropping patterns is shown in Table II. By formulating the appropriate rule set and counting the frequency of the characteristic signal of each pixel in the Sentinel dataset during different phenological windows, including $\text{SPSF}_{\text{PW}_n}$ (strong plant signal frequency in PW_n), $\text{WPSF}_{\text{PW}_n}$ (weak plant signal frequency), FSF_{PW_n} (flooding signal frequency), VSF_{PW_n} (vegetation signal frequency), and $\text{RFSF}_{\text{PW}_n}$ (rapeseed flowering signal frequency), only the pixels whose frequency of occurrence of this characteristic signal exceeds the corresponding threshold will be identified. The calculation formula is shown in Formulas (5)–(9) as follows. The validity of PW1, PW2, PW3, and images in 2020 are depicted in Fig. 5. According to the statistics shown in Figs. 3 and 4, the following specific phenological characteristic signal rules were determined:

1) Strong plant signal (SPS), NDVI > 0.75, LSWI > 0.3, NDVI > LSWI.
2) Weak plant signal (WPS), 0.3 < NDVI < 0.75, 0.2 < LSWI < 0.3, NDVI > LSWI.
3) Flooding signal (FS), LSWI > NDVI, VH < −24.
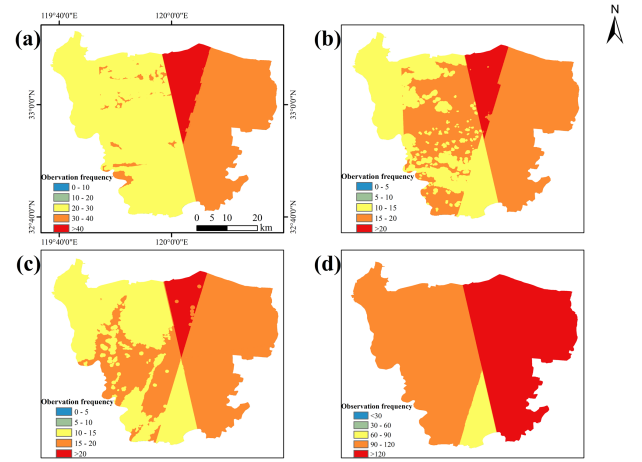4) Rapeseed flowering signal (RFS), VH > −15.

Fig. 5. Numbers of good-quality observations for individual pixels during the study period. (a) PW1. (b) PW2. (c) PW3. (d) 2020 whole year.

5) Vegetable signal (VS), RVI < 3, 0.2 < NDVI < 0.5, NDVI > LSWI

$$\text{SPSF}_{\text{PW}_n} = \frac{N_{\text{SPS in PW}_n}}{N_{\text{total in PW}_n}} \quad (5)$$

$$\text{WPSF}_{\text{PW}_n} = \frac{N_{\text{WPS in PW}_n}}{N_{\text{total in PW}_n}} \quad (6)$$

$$\text{FSF}_{\text{PW}_n} = \frac{N_{\text{Flooding in PW}_n}}{N_{\text{total in PW}_n}} \quad (7)$$

$$\text{VSF}_{\text{PW}_n} = \frac{N_{\text{Vegetation in PW}_n}}{N_{\text{total in PW}_n}} \quad (8)$$

$$\text{RFSF}_{\text{PW}_n} = \frac{N_{\text{RFS in PW}_n}}{N_{\text{total in PW}_n}} \quad (9)$$

where $N_{\text{SPS in PW}_n}$, $N_{\text{WPS in PW}_n}$, $N_{\text{Flooding in PW}_n}$, $N_{\text{Vegetation in PW}_n}$, $N_{\text{RFS in PW}_n}$ are the effective observation times of strong vegetation signal, weak vegetation signal, flooding signal, vegetable signal, and rapeseed flowering signal in PW_n, respectively. $N_{\text{total in PW}_n}$ is the number of effective observations of images in PW_n.

In order to ensure the accuracy of cropping patterns mapping, it is crucial to determine the threshold for the frequency of occurrence of different characteristic signals, which can avoid misclassification caused by the same characteristic signals that may briefly appear in different crops during the same season. Therefore, in this study, the frequency of the characteristic signals of the sample of different cropping patterns was counted in intervals with a step frequency of 0.05. The threshold value of the interval in which more than 95% of the sample points were located was selected, and this value was used as the threshold value to distinguish a certain cropping pattern within this phenological window. If there were relatively few outliers in the frequency distribution of the characteristic signal of the sample, the threshold was determined based on the critical value for the interval where the outliers were located.

D. RF Model

RF model, a popular machine learning model in recent years, has demonstrated exceptional performance in addressing classification and regression problems, making it a widely adopted approach in the field of remote sensing research [34], [35], [36]. RF model conducts classification through an ensemble of decision trees. This approach offers several advantages, including fast training speed, robust generalization ability, and model stability, making it a preferred choice in many applications [37]. Indeed, RF is generally more effective than other machine learning models in processing multisource remote sensing data and datasets with multidimensional variable features [38], [39]. Thus, we employed the RF model to map the cropping patterns. To ensure consistency with the variables used in the two methods, the RF classification was also executed in the GEE environment. The input data for the classification included optical images from three phenological windows (PW1, PW2, and PW3), radar images from two phenological windows (PW1 and PW2), and corresponding features such as NDVI, EVI, LSWI, RVI, and VH. The features inputted into the RF model include each vegetation index feature from each phenological window, as well as the maximum, minimum, and median values of the backscatter coefficient VH, totaling 42 features. The number of decision trees and feature sets are two important parameters of RF. In this study, we employed a random search strategy to determine the optimal number of decision trees and utilized the recursive feature elimination (RFE) algorithm [40] to refine the optimal feature set.

E. Accuracy Evaluation and Inter-Comparison

In this study, the training data and verification data were divided in a ratio of 6:4, and the classification results of the two different methods were evaluated using confusion matrix. Four evaluation metrics were calculated: overall accuracy (OA), kappa coefficient, producers' accuracy (PA), and users' accuracy (UA). Then, the method with higher classification accuracy was used for mapping cropping patterns in the study area.

IV. RESULTS

A. Threshold of RTM

The interval distribution of the characteristic signal frequencies of the main cropping patterns in the study area calculated based on sample points is illustrated in Fig. 6. Based on the threshold determination method described above, the threshold of $\text{SPSF}_{\text{PW}_1}$ and $\text{SPSF}_{\text{PW}_3}$ for mapping wheat-rice was 0.25 and 0.4, FSF_{PW_1} and $\text{SPSF}_{\text{PW}_3}$ for mapping crayfish-rice was 0.6 and 0.4, VSF_{PW_1} and $\text{SPSF}_{\text{PW}_3}$ for mapping vegetable-rice was 0.6 and 0.4, $\text{RFSF}_{\text{PW}_2}$ and $\text{SPSF}_{\text{PW}_3}$ for mapping rapeseed-rice was 0.6 and 0.4, $\text{RFSF}_{\text{PW}_2}$ and $\text{WPSF}_{\text{PW}_3}$ for mapping rapeseed-vegetable was 0.6 and 0.4, VSF_{PW_1} and $\text{WPSF}_{\text{PW}_3}$ for mapping year-round vegetables was 0.6 and 0.4.

B. Feature Selection of RF

In this study, the step size was set 5, and the classification accuracy was evaluated for different numbers of decision trees
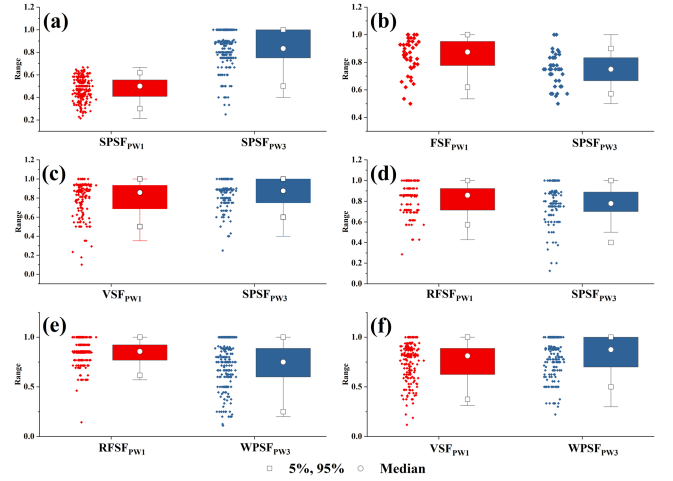

Fig. 6. Characteristic signal frequency distribution of main cropping patterns. (a) Wheat-rice. (b) Crayfish-rice. (c) Vegetable-rice. (d) Rice-rapeseed. (e) Rapeseed-vegetable. (f) Year-round vegetables.
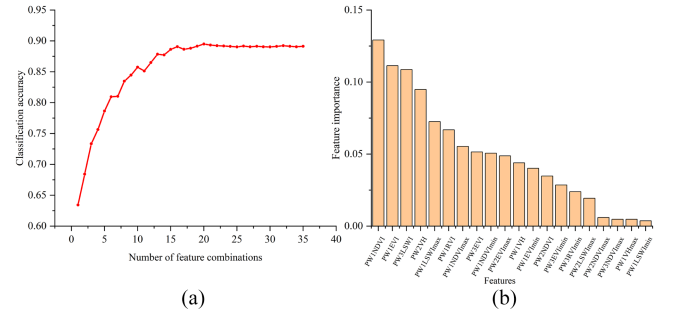

Fig. 7. Number of features and importance of each feature in the optimal feature set. (a) Relationship between classification accuracy and number of feature combinations. (b) Optimal features and their importance.

ranging from 1 to 1000. The highest accuracy was achieved at 45, 100, and 195 decision trees. To reduce training time, a decision tree number of 45 was chosen. In addition, too many features can lead to information redundancy and reduce classification accuracy [35]. Therefore, we used the RFE algorithm to filter the optimal feature set. First, seven feature indices with zero feature weights were eliminated using the Loss L1-regularized linear regression method, and then the relationship between the optimal number of feature sets and overall accuracy was plotted by RFE based on the remaining variables [see Fig. 7(a)]. The OA of the RF classification reached its maximum when the number of feature variables was 20, and the classification accuracy tends to stabilize as the number of features increases. Finally, the variables in the top 20 order of importance were renormalized [see Fig. 7(b)]. The top six scores were PW1NDVI, PW1EVI, PW3LSWI, PW2VH, PW1LSWImax, and PW1RVI. Combined with the phenology window, the importance of features in PW1 was generally greater than that in PW3 and PW2. This may be due to the relative complexity of crop types within PW1 and the fact that NDVI and EVI can significantly differentiate crop growth conditions, resulting in generally high importance scores. In addition, the importance of the median of the features
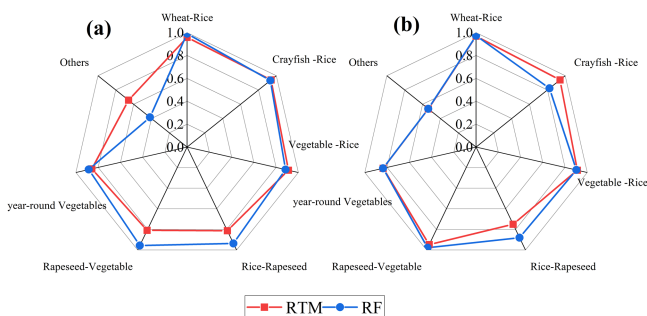
Fig. 8.   Comparison of accuracy of different cropping patterns. (a), (b) show the PA and UA of different cropping patterns, respectively.
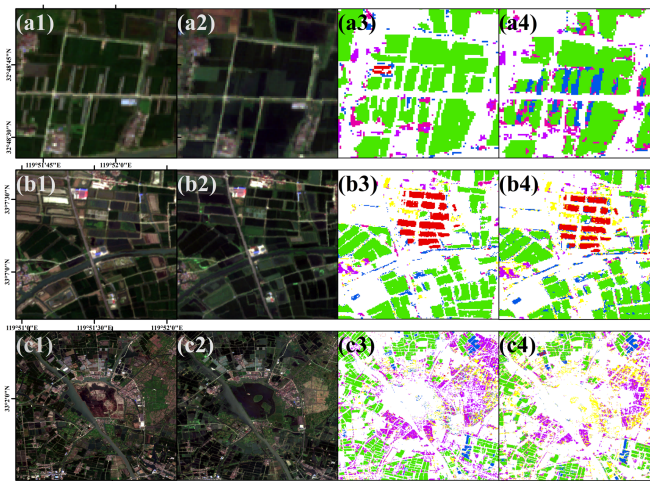

Fig. 9.   Classification details of RTM and RF. (a1)–(c1) True-color image of Sentinel in April 2020. (a2)–(c2) True color image of Sentinel in September 2020. (a3)–(c3) Classification results of RTM. (a4)-(c4) Classification results of RF.

in the phenology window was generally greater than the maximum and minimum of the features within the window. This suggests that using multidimensional feature variables can be more effective in mapping cropping patterns.

C. Accuracy Evaluation and Intercomparison

The accuracy of the RTM and the RF training results were verified using the confusion matrix. The OA of the RTM was 85.91%, with a Kappa coefficient of 0.831. The OA of the RF model was 89.50%, with a Kappa coefficient of 0.872. In terms of OA, the RF classification effect was slightly better than the RTM.

Comparing the accuracy of the two methods in different cropping patterns (see Fig. 8), it can be observed that the difference between the PA and the UA of the RTM and RF in wheat-rice and vegetable-rice mapping is small and they both perform well. The difference of PA between the two methods in crayfish-rice mapping was also small, but the UA of the RTM was 11.76% higher than that of RF. The PA and UA of RF in rapeseed-rice and rapeseed-vegetable were higher than those of the RTM by 12.36% and 13% and 14.76% and 3.04%, respectively. In addition, due to the diversity and fragmented distribution of vegetable types, both methods exhibited noticeable omissions and misclassifications in the mapping of year-round vegetables. We selected three typical regions to compare the classification results (see Fig. 9). It was observed that the RTM missed a portion of the vegetable-rice [see Fig. 9(a3)], while both methods mapped the crayfish-rice well [see Fig. 9(b3) and (b4)], with the RTM showing more completeness. However, the RF misclassified a portion of the rapeseed-vegetable pattern as year-round vegetables [see Fig. 9(c3) and (c4)]. Based on the classification accuracy of different cropping patterns, it could be observed that the RF performed better than the RTM in most cropping patterns, except for the crayfish-rice where the RTM showed higher accuracy.

D. Spatial Distribution of Cropping Patterns in Xinghua County

Comparing the classification effects of the two models, the RF method with higher accuracy was chosen to map the cropping patterns of the study area (see Fig. 10). Through the analysis of
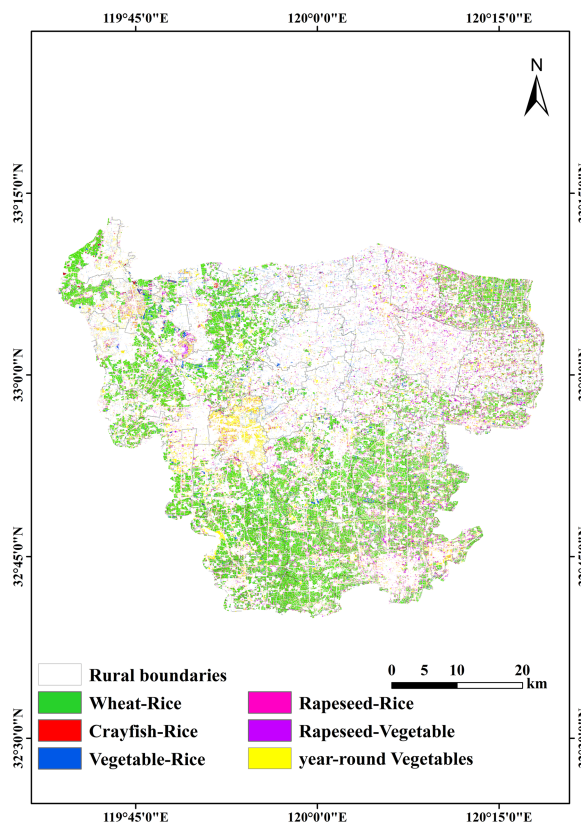

Fig. 10.   Spatial distribution map of cropping patterns.

the spatial distribution trends of several major crops, the distribution of cropping patterns in the study area and its influencing factors can be summarized into the following aspects:
1) Rice is the predominant crop in the study area, with its cultivation concentrated in the southern and northeastern regions. The rice fields are primarily utilized for wheat-rice rotation. In addition, the crayfish-rice, a newer
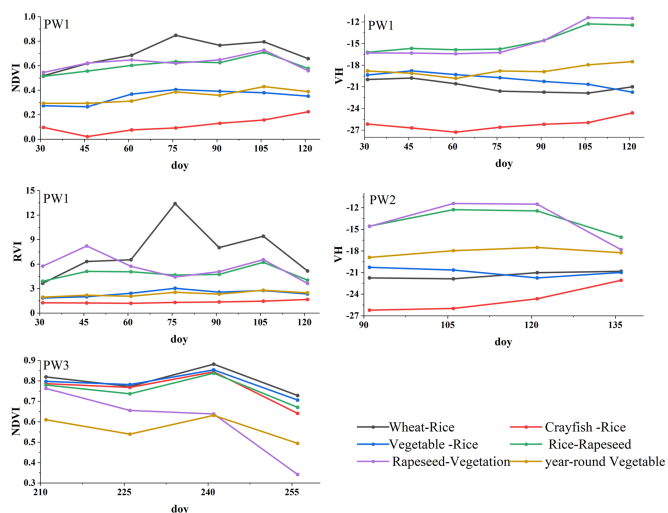
Fig. 11.　Characteristic curves of cropping patterns in phenological windows.

Fig. 12.　Maps of the two methods in 2020 and 2022.

ecological breeding approach, is predominantly concentrated in the northwestern part of the study area. Vegetable-rice and rapeseed-rice are relatively scattered and spread all over the whole area.

2) Rapeseed is the primary oil crop in the study area, typically grown in rapeseed-vegetable rotations. Its distribution is scattered, with concentrations near Centipede Lake and surrounding areas near the water system.

3) According to the research results and field survey, vegetables in the study area show a pattern of mainly aquatic vegetables in the northwest and mainly facility vegetables in the south.

V. DISCUSSION

A. Availability of PWF in Cropping Patterns Mapping

The division of phenological windows and the selection of features are crucial steps in constructing PWF. Therefore, this study separately analyzed the time-series curves of different cropping patterns within the phenological window to validate the reasonableness of using PWF (see Fig. 11). In PW1, the NDVI of wheat showed a significant increase compared to other winter crops. This is because after the overwintering period, wheat entered the greening stage, and its NDVI started to increase rapidly, reaching its maximum at the booting and heading stages. Due to the winter season, the growth of vegetables was relatively slow compared to other crops, and many vegetables, such as shallots and taro, were covered with plastic film or placed in greenhouses, resulting in a slow change in their NDVI values [41]. RVI is commonly utilized for detecting and estimating plant biomass owing to its sensitivity to the near-infrared band [42]. However, the presence of mulch film and greenhouses can weaken the vegetation signal of crops, resulting in spectral characteristics that resemble both soil covered with a small amount of vegetation and artificial ground surface [43]. This can lead to lower values of near-infrared band compared to crops such as wheat and rapeseed. The phenomenon also explains why
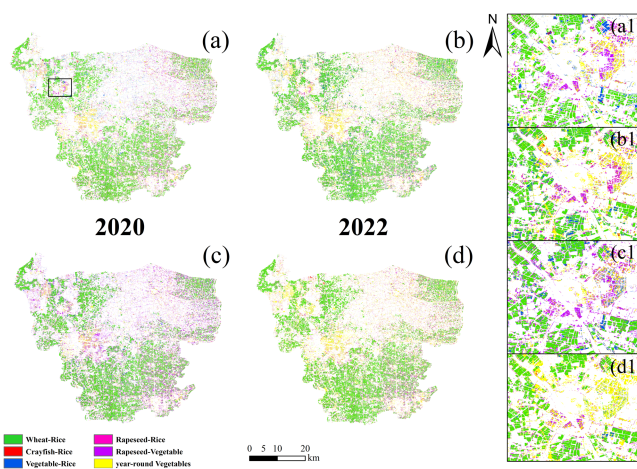
the RVI values for winter vegetables in PW1 remained relatively unchanged and at a low level. In addition, during the PW1, the crayfish-rice was typically in the stage of flooding and soaking fields, which can be easily identified by leveraging the sensitivity of SAR and LSWI to surface water [44]. In PW2, rapeseed entered flowering stage, and the VH value can distinguish well between rapeseed and other crops at this time. Some studies found rapeseed exhibits unique spectral and color differences during flowering [45]. And in similar studies, this period is frequently used as an entry point to map the spatial distribution of rapeseed by analyzing the photosynthetic parameters of the canopy [46], [47]. The NDVI of rice was much higher than that of vegetables during PW3. This is due to the fact that rice at this stage entered the booting and heading stages, and its chlorophyll content reached the peak, which is much higher than that of vegetables. Studies have shown that vegetation indices such as NDVI, EVI, and chlorophyll have a strong correlation, so that rice and vegetables can be distinguished by NDVI or EVI at this time. These indicated that the selection of PWF in this study aligned with crop growth trends and possessed a scientific foundation.

B. Advantages of PWF in Cropping Patterns Mapping

We applied the PWF to the data of 2022 and conducted a comparative analysis with the conventional RF method to assess the applicability of PWF. The maps obtained by the two methods are displayed in Fig. 12. Fig. 13 reveals that the method using PWF exhibited relatively higher accuracy. Additionally, PWF demonstrated consistent performance in other years, indicating its applicability. In Fig. 12(a1)–(d1), it is evident that traditional methods led to misclassifications in complex region, particularly in crops like vegetables. The main manifestations were that rapeseed-rice was mistakenly classified as rapeseed-vegetable and year-round vegetables were mistakenly identified as vegetable-rice and rapeseed-vegetable. This phenomenon may be attributed to the diversity of types of vegetables, undergoing substantial changes throughout their entire growth period, which poses a challenge in identifying them based on
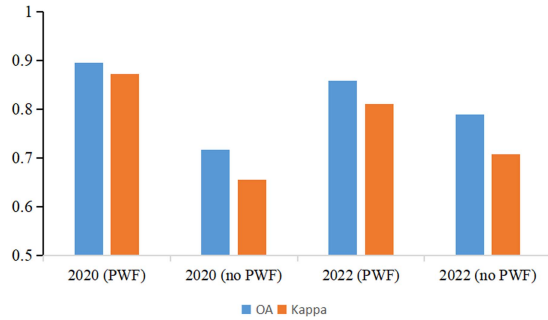
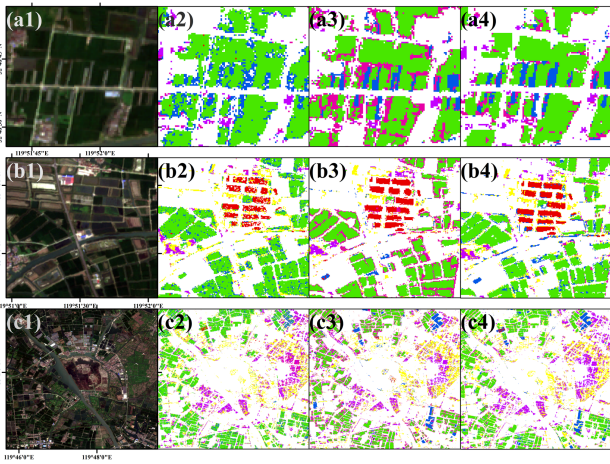Fig. 13. Comparison of different methods based on the PWF mapping accuracy.

Fig. 14. RF Classification details of only SAR and Optical variable characteristics. (a1)–(c1) True-color image of Sentinel in April 2020. (a2)–(c2) Classification results of only SAR variable characteristics. (a3)–(c3) Classification results of only optical variable characteristics. (a4)–(c4) Classification results of all variable characteristics.

a unified feature. Alternatively, the misclassification might be due to the classifier inputting characteristic variable information throughout the year, and the high similarity of certain crops at a specific growth stage overshadowing other classification information. The method with PWF effectively addressed this issue, relatively. By capturing the unique stages of crop growth and leveraging multidimensional feature information, it maximized the distinction between different cropping patterns and successfully reduced misclassification.

In addition, we also verified contribution of cooperative radar and optical images in cropping patterns mapping. This study used the RF method, which showed better classification results, as an example, and inputted separately the characteristic variables of SAR and optical images in the three phenological windows, while keeping the rest of the environment parameters unchanged. It was found that compared with inputting SAR alone and optical image features alone, the classification accuracy of collaborative SAR and optical image features increased by 13.66% and 3.62%, respectively. To emphasize the contrast, we selected the same typical area as shown in Fig. 9 to compare the classification results using single input SAR, optical image, and collaborative SAR and optical image features (see Fig. 14).

It is easy to find that the approach of combining SAR and optical image features collaboratively yields better results in RF classification. This also showed from the side that appropriate feature selection is conducive to improving mapping accuracy.

In summary, the PWF maximize the differences between different crops, and such differences are in accordance with the growth characteristics of the crop's critical fertility period and have a stronger physical interpretation in identifying different cropping patterns. In cases where the same cropping pattern exhibits significant temporal-spectral variability across different regions or years, it becomes necessary to reconstruct the time-spectrum curve of the typical cropping pattern. Subsequently, determining the number and window period of phenological windows based on the specific stages in the crop growth cycle enables more accurate mapping of cropping patterns. In their work, Han et al. [48] and Ibrahim et al. [49] successfully accomplished crop type mapping in expansive regions and over extended time scales through the appropriate time windows. This also demonstrates the feasibility of extracting cropping patterns in complex areas by choosing appropriate PWF. However, it should be acknowledged that the selection of PWF cannot be straightforwardly applied to other regions, and appropriate adjustments may be needed based on the environmental conditions of the study area.

C. Applicability of RTM and RF and Uncertainty Analysis of Cropping Patterns Mapping Result

This study utilized threshold methods and RF algorithms, which are widely used in current research, to construct different models, all of which yielded favorable classification results. Among these methods, the RTM demonstrates robust generalization ability, and the selected key features possess a strong physical interpretation. In addition, this method exhibits low dependency on sample size, making it suitable for generalization and application on larger spatial and temporal scales. However, the RTM requires strong prior knowledge and may need different rule sets to be determined for different regions based on factors such as climate and crop type. As a machine learning model, the RF has the advantage of fast training speed. Moreover, when the same set of phenological characteristic variables is input, the RF tends to yield slightly better classification results compared to the RTM. But it also requires an accurate and sufficient sample sets to support the training model. In addition, the study area is characterized by low relief and flat terrain. To ensure the consistency of the two methods, texture and topographic features were not taken into account in this study. It has been shown that incorporating suitable texture and terrain features can improve the classification results to some extent [50]. At the same time, different models may perform differently in different environmental conditions. Therefore, it is crucial to carefully select an appropriate classification model based on the specific local conditions for optimal results in the areas with complex cropping patterns.

Despite the good classification results, this study still has some shortcomings to be improved. First, in order to mitigate the influence of factors such as forest land, this study was

conducted on the basis of the cropland layer. To accurately delineate cultivated land, this study employed the RF method to classify the land cover type into five categories: cultivated land, forest, water, building, and others. The OA of the classification was 91.84%, with the PA of 93.12% and the UA of 92.34% specifically for cultivated land. Although the range of cultivated land was mapped more accurately, the results of cropping pattern mapping will inevitably be affected by the accuracy of cultivated land mapping. In addition, pixel-based research is susceptible to "salt and pepper noise" interference [18], and the classification details may be relatively fragmented. In this article, it was mainly observed in the relatively fragmented vegetable land. When counting the specific area of different cropping patterns, the result may be too large. In the future, object-oriented approaches or studies at the plot scale can be considered for follow-up.

VI. Conclusion

The development of satellites with high spatial and temporal resolution has made it possible to create fine-scale cropping pattern maps in agriculturally intensive areas with fragmented agriculture fields. In this study, a novel feature was proposed that combines SAR and optical images with PWF for the successful mapping of the spatial distribution of cropping patterns in Xinghua County. The main steps include the following:

1) Compositing half-moon images to construct VIs and VH standard time-series curves of different cropping patterns.
2) Determining the phenological window.
3) Using the RTM and RF to map the cropping patterns.

The results of the study showed that the phenological windows extracted from the cropping patterns in the study area were 30–120, 90–135, and 200–270 days, respectively. The OA of RTM and RF, based on phenological window features, were 85.91% and 89.50%, respectively. The kappa coefficients for RTM and RF were 0.831 and 0.872, respectively. In terms of classification performance, RF slightly outperformed RTM. The PWF proposed in this study can effectively identify cropping patterns in agriculturally intensive areas, which can provide valuable data for ecosystem service assessment and regional landscape planning.

References

[1] Y. Lang and W. Song, "Quantifying and mapping the responses of selected ecosystem services to projected land use changes," *Ecological Indicators*, vol. 102, pp. 186–198, Jul. 2019, doi: 10.1016/j.ecolind.2019.02.019.

[2] C. N. M. Deloyde and W. E. Mabee, "Ecosystem service values as an ecological indicator for land management decisions: A case study in southern Ontario, Canada," *Ecological Indicators*, vol. 151, Jul. 2023, Art. no. 110344, doi: 10.1016/j.ecolind.2023.110344.

[3] Y. Su et al., "Patterns and controls of ecosystem service values under different land-use change scenarios in a mining-dominated basin of northern China," *Ecological Indicators*, vol. 151, Jul. 2023, Art. no. 110321, doi: 10.1016/j.ecolind.2023.110321.

[4] M. Li et al., "Crop rotation history constrains soil biodiversity and multifunctionality relationships," *Agriculture, Ecosyst. Environ.*, vol. 319, Oct. 2021, Art. no. 107550, doi: 10.1016/j.agee.2021.107550.

[5] D. G. Bullock, "Crop rotation," *Crit. Rev. Plant Sci.*, vol. 11, no. 4, pp. 309–326, Jan. 1992, doi: 10.1080/07352689209382349.

[6] S. T. Rosenzweig, M. E. Stromberger, and M. E. Schipanski, "Intensified dryland crop rotations support greater grain production with fewer inputs," *Agriculture, Ecosyst. Environ.*, vol. 264, pp. 63–72, Sep. 2018, doi: 10.1016/j.agee.2018.05.017.

[7] M. Kiani et al., "Quantifying sensitive soil quality indicators across contrasting long-term land management systems: Crop rotations and nutrient regimes," *Agriculture, Ecosyst. Environ.*, vol. 248, pp. 123–135, Oct. 2017, doi: 10.1016/j.agee.2017.07.018.

[8] J. A. Martínez-Casasnovas, A. Martín-Montero, and M. Auxiliadora Casterad, "Mapping multi-year cropping patterns in small irrigation districts from time-series analysis of Landsat TM images," *Eur. J. Agronomy*, vol. 23, no. 2, pp. 159–169, Sep. 2005, doi: 10.1016/j.eja.2004.11.004.

[9] Y. Liu, Q. Yu, Q. Zhou, C. Wang, S. D. Bellingrath-Kimura, and W. Wu, "Mapping the complex crop rotation systems in Southern China considering cropping intensity, crop diversity, and their seasonal dynamics," *IEEE J. Sel. Topics Appl. Earth Observ. Remote Sens.*, vol. 15, pp. 9584–9598, 2022, doi: 10.1109/JSTARS.2022.3218881.

[10] M. Mahlayeye, R. Darvishzadeh, and A. Nelson, "Cropping patterns of annual crops: A remote sensing review," *Remote Sens.*, vol. 14, no. 10, pp. 90–753, May 2022.

[11] J. Adrian, V. Sagan, and M. Maimaitijiang, "Sentinel SAR-optical fusion for crop type mapping using deep learning and Google Earth Engine," *Int. Soc. Photogrammetry Remote Sens.-J. Photogrammetry Remote Sens.*, vol. 175, pp. 215–235, May 2021, doi: 10.1016/j.isprsjprs.2021.02.018.

[12] G. Li et al., "Crop type mapping using time-series Sentinel-2 imagery and U-Net in early growth periods in the Hetao irrigation district in China," *Comput. Electron. Agriculture*, vol. 203, Dec. 2022, Art. no. 107478, doi: 10.1016/j.compag.2022.107478.

[13] D. Ashourloo, H. S. Shahrabi, M. Azadbakht, A. M. Rad, H. Aghighi, and S. Radiom, "A novel method for automatic potato mapping using time series of Sentinel-2 images," *Comput. Electron. Agriculture*, vol. 175, Aug. 2020, Art. no. 105583, doi: 10.1016/j.compag.2020.105583.

[14] Y. Chen et al., "Mapping croplands, cropping patterns, and crop types using MODIS time-series data," *Int. J. Appl. Earth Observ. Geoinf.*, vol. 69, pp. 133–147, Jul. 2018, doi: 10.1016/j.jag.2018.03.005.

[15] M. Weiss, F. Jacob, and G. Duveiller, "Remote sensing for agricultural applications: A meta-review," *Remote Sens. Environ.*, vol. 236, Jan. 2020, Art. no. 111402, doi: 10.1016/j.rse.2019.111402.

[16] A. Tariq, J. Yan, A. S. Gagnon, M. R. Khan, and F. Mumtaz, "Mapping of cropland, cropping patterns and crop types by combining optical remote sensing images with decision tree classifier and random forest," *Geo-Spatial Inf. Sci.*, vol. 26, pp. 302–319, 2022, doi: 10.1080/10095020.2022.2100287.

[17] J. Ye, C. Wang, H. Gao, H. Fan, T. Song, and L. Ding, "A novel unsupervised object-level crop rotation detection with time-series dual-polarimetric SAR data," *IEEE Geosci. Remote Sens. Lett.*, vol. 19, 2022, Art. no. 4511905, doi: 10.1109/LGRS.2022.3195809.

[18] S. Ma, D. Wang, H. Yang, H. Hou, C. Li, and Z. Li, "A Bi-temporal-feature-difference- and object-based method for mapping rice-crayfish fields in Sihong, China," *Remote Sens.*, vol. 15, no. 3, Jan. 2023, Art. no. 658, doi: 10.3390/rs15030658.

[19] G. Waldhoff, U. Lussem, and G. Bareth, "Multi-data approach for remote sensing-based regional crop rotation mapping: A case study for the Rur catchment, Germany," *Int. J. Appl. Earth Observ. Geoinf.*, vol. 61, pp. 55–69, Sep. 2017, doi: 10.1016/j.jag.2017.04.009.

[20] H. Xing, B. Chen, and M. Lu, "A sub-seasonal crop information identification framework for crop rotation mapping in smallholder farming areas with time series Sentinel-2 imagery," *Remote Sens.*, vol. 14, no. 24, Dec. 2022, Art. no. 6280, doi: 10.3390/rs14246280.

[21] L. Liu et al., "Mapping cropping intensity in China using time series Landsat and Sentinel-2 images and Google Earth Engine," *Remote Sens. Environ.*, vol. 239, Mar. 2020, Art. no. 111624, doi: 10.1016/j.rse.2019.111624.

[22] Z. Yang et al., "What drives the spatial heterogeneity of cropping patterns in the Northeast China: The natural environment, the agricultural economy, or policy?," *Sci. Total Environ.*, vol. 905, Dec. 2023, Art. no. 167810, doi: 10.1016/j.scitotenv.2023.167810.

[23] Y. Liu, W. Zhao, S. Chen, and T. Ye, "Mapping crop rotation by using deeply synergistic optical and SAR time series," *Remote Sens.*, vol. 13, no. 20, Jan. 2021, Art. no. 4160, doi: 10.3390/rs13204160.

[24] R. Li et al., "Phenology-based classification of crop species and rotation types using fused MODIS and Landsat data: The comparison of a random-forest-based model and a decision-rule-based model," *Soil Tillage Res.*, vol. 206, Feb. 2021, Art. no. 104838, doi: 10.1016/j.still.2020.104838.

[25] T. Ren, H. Xu, X. Cai, S. Yu, and J. Qi, "Smallholder crop type mapping and rotation monitoring in mountainous areas with Sentinel-1/2 imagery," *Remote Sens.*, vol. 14, no. 3, Jan. 2022, Art. no. 566, doi: 10.3390/rs14030566.

[26] Z. Ma et al., "A framework combined stacking ensemble algorithm to classify crop in complex agricultural landscape of high altitude regions with Gaofen-6 imagery and elevation data," *Int. J. Appl. Earth Observ. Geoinf.*, vol. 122, Aug. 2023, Art. no. 103386, doi: 10.1016/j.jag.2023.103386.

[27] S. Liu, Z. Zhou, H. Ding, Y. Zhong, and Q. Shi, "Crop mapping using sentinel full-year dual-polarized SAR data and a CPU-optimized convolutional neural network with two sampling strategies," *IEEE J. Sel. Topics Appl. Earth Observ. Remote Sens.*, vol. 14, pp. 7017–7031, 2021, doi: 10.1109/JSTARS.2021.3094973.

[28] D. Mandal et al., "Dual polarimetric radar vegetation index for crop growth monitoring using Sentinel-1 SAR data," *Remote Sens. Environ.*, vol. 247, Sep. 2020, Art. no. 111954, doi: 10.1016/j.rse.2020.111954.

[29] Y. Wang, Z. Zhang, L. Feng, Y. Ma, and Q. Du, "A new attention-based CNN approach for crop mapping using time series Sentinel-2 images," *Comput. Electron. Agriculture*, vol. 184, May 2021, Art. no. 106090, doi: 10.1016/j.compag.2021.106090.

[30] L. Pan et al., "Mapping cropping intensity in Huaihe basin using phenology algorithm, all Sentinel-2 and Landsat images in Google Earth Engine," *Int. J. Appl. Earth Observ. Geoinf.*, vol. 102, Oct. 2021, Art. no. 102376, doi: 10.1016/j.jag.2021.102376.

[31] J. Tao, W. Wu, Y. Zhou, Y. Wang, and Y. Jiang, "Mapping winter wheat using phenological feature of peak before winter on the North China Plain based on time-series MODIS data," *J. Integrative Agriculture*, vol. 16, no. 2, pp. 348–359, Feb. 2017, doi: 10.1016/S2095-3119(15)61304-1.

[32] P. V. Arun and A. Karnieli, "Augmentation of vegetation index curves considering the crop-specific phenological characteristics," *IEEE J. Sel. Topics Appl. Earth Observ. Remote Sens.*, vol. 15, pp. 1235–1243, 2022, doi: 10.1109/JSTARS.2022.3142395.

[33] J. Dong et al., "Mapping paddy rice planting area in northeastern Asia with Landsat 8 images, phenology-based algorithm and Google Earth Engine," *Remote Sens. Environ.*, vol. 185, pp. 142–154, Nov. 2016, doi: 10.1016/j.rse.2016.02.016.

[34] M. Belgiu and L. Drăguţ, "Random forest in remote sensing: A review of applications and future directions," *Int. Soc. Photogrammetry Remote Sens., J. Photogrammetry Remote Sens.*, vol. 114, pp. 24–31, Apr. 2016, doi 10.1016/j.isprsjprs.2016.01.011.

[35] M. H. R. Sales, S. de Bruin, C. Souza, and M. Herold, "Land use and land cover area estimates from class membership probability of a random forest classification," *IEEE Trans. Geosci. Remote Sens.*, vol. 60, 2022, Art. no. 4402711, doi: 10.1109/TGRS.2021.3080083.

[36] A. Fallatah, S. Jones, and D. Mitchell, "Object-based random forest classification for informal settlements identification in the Middle East: Jeddah a case study," *Int. J. Remote Sens.*, vol. 41, no. 11, pp. 4421–4445, Jun. 2020, doi: 10.1080/01431161.2020.1718237.

[37] L. Breiman, "Random forests," *Mach. Learn.*, vol. 45, no. 1, pp. 5–32, Oct. 2001, doi: 10.1023/A:1010933404324.

[38] J. L. Speiser, M. E. Miller, J. Tooze, and E. Ip, "A comparison of random forest variable selection methods for classification prediction modeling," *Expert Syst. Appl.*, vol. 134, pp. 93–101, Nov. 2019, doi: 10.1016/j.eswa.2019.05.028.

[39] M. Sheykhmousa, M. Mahdianpari, H. Ghanbari, F. Mohammadimanesh, P. Ghamisi, and S. Homayouni, "Support vector machine versus random forest for remote sensing image classification: A meta-analysis and systematic review," *IEEE J. Sel. Topics Appl. Earth Observ. Remote Sens.*, vol. 13, pp. 6308–6325, 2020, doi: 10.1109/JSTARS.2020.3026724.

[40] M. Belgiu and O. Csillik, "Sentinel-2 cropland mapping using pixel-based and object-based time-weighted dynamic time warping analysis," *Remote Sens. Environ.*, vol. 204, pp. 509–523, Jan. 2018, doi: 10.1016/j.rse.2017.10.005.

[41] S. Foerster, K. Kaden, M. Foerster, and S. Itzerott, "Crop type mapping using spectral–temporal profiles and phenological information," *Comput. Electron. Agriculture*, vol. 89, pp. 30–40, Nov. 2012, doi: 10.1016/j.compag.2012.07.015.

[42] A. I. de Castro, M. Jurado-Expósito, J. M. Peña-Barragán, and F. López-Granados, "Airborne multi-spectral imagery for mapping cruciferous weeds in cereal and legume crops," *Precis. Agriculture*, vol. 13, no. 3, pp. 302–321, Jun. 2012, doi: 10.1007/s11119-011-9247-0.

[43] A. Ma, D. Chen, Y. Zhong, Z. Zheng, and L. Zhang, "National-scale greenhouse mapping for high spatial resolution remote sensing imagery using a dense object dual-task deep learning framework: A case study of China," *Int. Soc. Photogrammetry Remote Sens., J. Photogrammetry Remote Sens.*, vol. 181, pp. 279–294, Nov. 2021, doi: 10.1016/j.isprsjprs.2021.08.024.

[44] R. Nasirzadehdizaji, Z. Cakir, F. Balik Sanli, S. Abdikan, A. Pepe, and F. Calò, "Sentinel-1 interferometric coherence and backscattering analysis for crop monitoring," *Comput. Electron. Agriculture*, vol. 185, Jun. 2021, Art. no. 106118, doi: 10.1016/j.compag.2021.106118.

[45] J. Tao, X. Zhang, Q. Wu, and Y. Wang, "Mapping winter rapeseed in South China using Sentinel-2 data based on a novel separability index," *J. Integrative Agriculture*, vol. 22, pp. 1645–1657, Oct. 2022, doi: 10.1016/j.jia.2022.10.008.

[46] Y. Zang et al.., "Mapping rapeseed in China during 2017-2021 using Sentinel data: An automated approach integrating rule-based sample generation and a one-class classifier (RSG-OC)," *GIScience Remote Sens.*, vol. 60, no. 1, Dec. 2023, Art. no. 2163576, doi: 10.1080/15481603.2022.2163576.

[47] S. Zhang, X. Kang, and S. Li, "Phenology-based unsupervised rapeseed mapping using multitemporal data," *IEEE J. Sel. Topics Appl. Earth Observ. Remote Sens.*, vol. 15, pp. 9809–9820, 2022, doi: 10.1109/JSTARS.2022.3217665.

[48] J. Han et al., "Prediction of winter wheat yield based on multi-source data and machine learning in China," *Remote Sens.*, vol. 12, no. 2, Jan. 2020, Art. no. 236, doi: 10.3390/rs12020236.

[49] E. S. Ibrahim, P. Rufin, L. Nill, B. Kamali, C. Nendel, and P. Hostert, "Mapping crop types and cropping systems in Nigeria with Sentinel-2 imagery," *Remote Sens.*, vol. 13, no. 17, 2021, Art. no. 3523, doi: 10.3390/rs13173523.

[50] K. Luo, L. Lu, Y. Xie, F. Chen, F. Yin, and Q. Li, "Crop type mapping in the central part of the North China plain using Sentinel-2 time series and machine learning," *Comput. Electron. Agriculture*, vol. 205, Feb. 2023, Art. no. 107577, doi: 10.1016/j.compag.2022.107577.
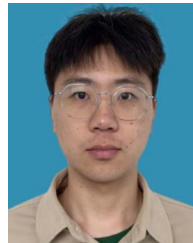
Haichao Yang received the bachelor's degree in land resources management from Henan Agricultural University, Zhengzhou, China, in 2021. He is currently working toward the master's degree in pedology in Nanjing Agricultural University, Nanjing, China.

His research interests include remote sensing of agriculture, especially spaceborne remote sensing analysis for monitoring and mapping cropland use.

Danyang Wang received the bachelor's degree in land resources management and the master's degree in agricultural engineering and technology from Shandong Agricultural University, Tai'an, China, in 2018 and 2020, respectively. She is currently working toward the Ph.D. degree in agricultural resources and environment with the Nanjing Agricultural University, Nanjing, China.

Her research interests include remote sensing, and machine learning, especially spaceborne remote sensing analysis for monitoring and mapping cropland use.

Jingda Xin received the bachelor's degree in surveying engineering from Jilin Jianzhu University, Changchun, China, in 2019, and the master's degree in remote sensing of resources and environment from Yunnan Agricultural University, Kunming, China, in 2022.

His research interests include remote sensing, and machine learning, especially spaceborne remote sensing analysis for monitoring and mapping cropland use.

Hao Qian was born in Taizhou, Jiangsu, China, in 1999. He received the bachelor's degree in agriculture from Nanjing Agricultural University, Nanjing, China, in 2021, where he is currently working toward the master's degree in soil science with Nanjing Agricultural University.

His research interests include remote sensing and ecosystem service assessment.

Cheng Li received the doctoral degree in cartography and geographical information system from the Institute of Geographic Sciences and Natural Resources Research, Chinese Academy of Sciences, Beijing, China, in 2022.

He is currently a Postdoc in agricultural resources and environment with the Nanjing Agricultural University, Nanjing, China. His research interests include remote sensing of ecological environment and agriculture.

Yunqi Wang received the bachelor's degree in land resources management from Henan Agricultural University, Zhengzhou, China, in 2021. He is currently working toward the master's degree in pedology in Nanjing Agricultural University, Nanjing, China.

His research interests include agricultural remote sensing and unmanned aerial vehicle remote sensing for soil fertility inversion.

Yayi Tan received the bachelor's degree in agricultural resources and environment from Nanjing Agriculture University, Nanjing, China, in 2022, where she is currently working toward the master's degree in soil remote sensing.

Her research interests include remote sensing, and soil science, especially satellite remote sensing analysis for land use and dynamics of soil organic carbon.

Jingyu Dai received the Ph.D. degree in agricultural resources and environment from Kyoto Prefectural University, Kyoto, Japan, in 2000.

He is currently a Professor with Nanjing Agricultural University, Nanjing, China. His current research interests include natural organic matter chemistry in the environment and pollution control chemistry.

Haiyan Zhao received the master's degree in soil science from Nanjing Agricultural University, Nanjing, China, in 2004.

She is currently an Associate with Nanjing Agricultural University, Nanjing, China. She works as a Senior Experimentalist in the College of Resource and Environmental Sciences.

Zhaofu Li received the bachelor's of science degree from the Northeast Institute of Geography and Agroecology, Chinese Academy of Sciences, Beijing, China, in 2002, and the Ph.D. degree in physical geography from the Nanjing Institute of Geography and Limnology, Chinese Academy of Sciences, Beijing, in 2006.

His main research interests include soil resources and information technology, land use change and resource and environmental effects, agricultural nonpoint source pollution model, and application of remote sensing and geographic information system in resource and environmental science.